TABLE I. Parameters of Callaway's model giving the best fit to the experimental data.

	A_{exp} (10^{-43} sec^3)	$(B_1+B_2)_{exp}$ (sec deg^{-3})	$(c/L)_{exp}$ (10^7 sec^{-1})	A_{cal} (10^{-43} sec^3)	A_{exp}/A_{cal}	$(c/L)_{exp}/(c/L)_{cal}$
1. Silicon	0.05	5×10^{-24}	0.214	0.033	1.5	1.0
2. Diamond	0.021	2×10^{-25}	0.268	2.1×10^{-4}	100	1.0
3. Solid argon	4.01	8×10^{-19}	130	4.01	1.0	2.6×10^{4}
4. Solid neon	29.32	3.5×10^{-18}	10	29.32	1.0	1.6×10^{3}
5. KCl	1.97	1.2×10^{-21}	0.025	1.31	1.5	1.0
6. NaF	...	1×10^{-22}	0.7	...	...	4.7

Umklapp processes are predominant at the conductivity maximum. In diamond, where the Debye temperature is quite high and Umklapp processes are unimportant at the temperatures of interest, the results of both the models are more or less similar.

(2) Casimir's model for the determination of the characteristic length for boundary relaxation time $\tau_B = L/c$ fails to explain the observed results in solidified argon and neon. This indicates the existence of microscale fluctuations in the composition of the solid. In NaF too, the calculations indicate that there exist internal boundaries, associated with fluctuations.

(3) The value of the parameter A for the isotopic scattering time $1/\tau_P = A\omega^4$, which explains the experimental results in diamond, is a hundred times the value calculated from Klemens' formula. This supports the earlier suggestion that in diamond there occur groups or clusters which result in the increased value of A.

(4) The assumption that the parameter (B_1+B_2) is temperature independent, gives approximately a good fit to the experimental curve in all the cases.

In Casimir's theory the scattering of phonons is completely diffuse, the incident phonons being absorbed and then re-emitted with the equilibrium distribution corresponding to local temperature. The temperature is assumed to be so low that the only collisions made by the phonons are with the boundary. Boundary scattering does not occur uniformly throughout the crystal, which makes the distribution function depend upon position. The phonons are also scattered by other defects and by each other. Assuming that there is specular reflection of the phonons and that there exists an equivalent relaxation time which includes the effect of normal processes, and proceeding directly from the Boltzmann equation, attempts[23,5] have been made to find an expression for the effective boundary relaxation time. Specular reflection leads to an increased value of the boundary relaxation time τ_B. However, for solid argon and neon and NaF, in order to explain the experimental results we require increased values of c/L, which means the existence of internal boundaries.

ACKNOWLEDGMENT

The authors would like to express their thanks to Professor K. S. Singwi for helpful discussions.

[23] C. Herring, Phys. Rev. **96**, 1163 (1954).

PHYSICAL REVIEW VOLUME 126, NUMBER 1 APRIL 1, 1962

Scattering of Slow Neutrons by Solid and Liquid Terphenyls*

ROBERT M. BRUGGER
Atomic Energy Division, Phillips Petroleum Company, Idaho Falls, Idaho

(Received November 22, 1961)

The partial differential cross sections for scattering of slow neutrons by samples of solid and liquid terphenyls were measured and are presented in scattering law form. These data show that the difference between the scattering from the liquid and the solid is principally of magnitude and not shape. No effects due to the ortho-, meta-, or para-chemical binding is evident. Resonances attributed to transitions between vibrational states in the molecule are seen in the liquid data but not in the solid data. Fourier inversion of the scattering-law data show that the space-time self-correlation function $G_s(\bar{r},t)$ for these materials is not Gaussian. A comparison of these data with other available scattering-law curves indicate that the curves may be grouped into classes of (1) polycrystalline solids, (2) liquid–amorphous solids, and (3) gases. The total cross sections for the terphenyls for 0.0251 ev neutrons were also measured.

A. INTRODUCTION

SLOW neutron inelastic scattering data are rapidly becoming available that reveal the extensive properties and details of the solid, liquid, and gaseous states. The inelastic neutron scattering from methane gas[1] and from propane gas[2] have been measured using the MTR

* Work done under the auspices of the U. S. Atomic Energy Commission.

[1] P. D. Randolph, R. M. Brugger, K. A. Strong and R. E. Schmunk, Phys. Rev. **124**, 460 (1961).
[2] K. A. Strong, G. D. Marshall, R. M. Brugger and P. D. Randolph, Phys. Rev. **125**, 933 (1962).

phased-chopper velocity selector. The scattering from liquid lead[3] has been measured using the Chalk River triple-axis spectrometer. The scattering from H_2O, D_2O,[4] and graphite[5] have been measured by means of the Chalk River-Harwell velocity selector. Extensive measurements of this type are important, not only because they reveal physical properties that have not been obtained by other methods, but because they provide an understanding of moderation of neutrons as they near thermal energies.

To continue these studies, the terphenyls (molecules of three joined benzene rings) were selected as samples for extensive inelastic scattering measurements using the MTR velocity selector.[6] Scattering measurements were made at angles from 16° to 85° to the incident neutron beam and at initial energies between 0.01 and 0.1 ev. Total cross sections for the samples for 0.0251-ev neutrons were also obtained for normalizing the scattering cross sections. Data for solid ortho-, meta-, and para-terphenyl and for both solid and liquid Santowax-R were obtained. Santowax-R is a mixture of the three terphenyls. The terphenyls were selected for study because (1) they are principally incoherent scatterers, thus eliminating the problem of extracting the coherent scattering before studying the non-nuclear properties of the sample, (2) samples of both the solid and liquid are easily made, (3) measurements of the liquid and solid states might indicate relations between these two states (4) the effect of the ortho-, meta-, or para-chemical bonding might be evident, and (5) knowledge of the moderating properties of terphenyls (the principle organic moderator now used) is important for reactor technology.

Examples of the data are presented in absolute units as partial differential cross sections and the complete data as scattering law $S(\alpha,\beta)$.[7] The partial differential cross sections, the direct experimental data obtained, is the more familiar presentation. The scattering-law presentation is more convenient for flux moderation calculations and for physical interpretation because the detailed-balance factor is extracted[8] and because the data are overdetermined and intermixed. In the scattering-law presentation of the data, the energy change is represented through $\beta=\hbar\omega/K_BT$, where $\hbar$ is Planck's constant divided by 2π, $\hbar\omega$ is the energy change, K_B is Boltzmann's constant, and T is the absolute temperature of the sample. Momentum change is represented through $\alpha=\hbar^2\kappa^2/2MK_BT$, where $\bar{\kappa}=\bar{k}-\bar{k}_0$, with $\bar{k}$ and $\bar{k}_0$ the final and initial wave vector of the neutron, respectively.

In the data there are no observable differences that can be attributed to the ortho-, meta-, or para-chemical bonds. The differences between the solid and the liquid data are principally of magnitude and not shape.

The liquid Santowax-R data show evidence for energy transitions between states in the molecule of about 0.1 and 0.2 ev while the solid data give no indication of these transitions. These transitions are probably caused by vibrational modes in the aromatic ring that have large amplitudes for hydrogen motion.

From the available $S(\alpha,\beta)$ data for different types of samples,[9] there are indications of characteristic shapes for classes of material. The suggested classes are (1) polycrystalline solids, (2) liquid–amorphous solids, and (3) gases. Both the solid and liquid terphenyl data have the liquid–amorphous solid shape.

The interpretation of slow-neutron inelastic scattering data is in its infancy. Only for methane have the scattering data been satisfactorily explained[1,10] by a theory incorporating the known basic physical properties (the rotational and vibrational level spacings) of the sample. Brockhouse[3] applied double Fourier transformations to his liquid lead data to obtain the space-time correlation function of Van Hove,[11] a function more amenable to theory. Egelstaff,[4,5] instead of applying Fourier transformations in analyzing his H_2O, D_2O, and graphite data, fits trial theoretical curves to his $S(\alpha,\beta)$ data and extrapolated $S(\alpha,\beta)/\alpha$ to small values of α to obtain a function related to the velocity correlation function.[12] Interpretations of the terphenyl data by both double Fourier transformations and extrapolation of $S(\alpha,\beta)/\alpha$ were considered and rejected.

Modifications of an interpretation by single Fourier transformation suggested by Vineyard[13] and Rahman[14] were tried. The resulting intermediate function $\gamma(\bar{\kappa},t)$ is not the Gaussian form $\exp[-\kappa^2\rho(t)/2]$ predicted with $\rho(t)$ a function of t only but is more nearly $\exp[-(\kappa^2+1)\rho(t)_1]$ at large α and $\exp[-\kappa\rho(t)_2]$ at small α. However, these modifications still do not give good representations of the data, especially where discrete energy transitions in the molecule are evident.

The data indicate that per hydrogen atom liquid Santowax-R is as good a thermal moderator as is water. Attempts to extrapolate the $S(\alpha,\beta)$ data to larger α

[3] B. N. Brockhouse and N. K. Pope, Phys. Rev. Letters **3**, 259 (1959).

[4] P. A. Egelstaff, S. J. Cocking, R. J. Royston, and I. M. Thorson, *International Atomic Energy Agency Symposium on Inelastic Scattering of Neutrons in Solids and Liquids, Vienna, Austria, October 11–14, 1960* [International Atomic Energy Agency (to be published)], Paper IS/10.

[5] P. A. Egelstaff and S. J. Cocking, *International Atomic Energy Agency Symposium on Inelastic Scattering of Neutrons in Solids and Liquids, Vienna, Austria, October 11–14, 1960* [International Atomic Energy Agency (to be published)], Paper IS/8.

[6] R. M. Brugger and J. E. Evans, Nuclear Instr. and Methods **12**, 75 (1961).

[7] P. A. Egelstaff, *International Atomic Energy Agency Symposium on Inelastic Scattering of Neutrons in Solids and Liquids, Vienna, Austria, October 11–14, 1960.* [International Atomic Energy Agency (to be published)]. Paper IS/7.

[8] P. Schofield, Phys. Rev. Letters **4**, 239 (1960).

[9] R. M. Brugger, U. S. Atomic Energy Commission Report IDO-16699, 1961 (unpublished).

[10] G. W. Griffing, Phys. Rev. **124**, 1489 (1961).

[11] L. Van Hove, Phys. Rev. **95**, 249 (1954).

[12] P. A. Egelstaff, Nuclear Sci. and Eng. **12**, 250 (1962); P. A. Egelstaff & P. Scofield, *ibid.* **12**, 260 (1962).

[13] G. H. Vineyard, Phys. Rev. **110**, 999 (1958).

[14] A. Rahman, K. S. Singwi and A. Sjölander, Phys. Rev. **122**, 9 (1961).

TABLE 1. Properties of solid terphenyl samples.

Sample	% ortho-terphenyl	% meta-terphenyl	% para-terphenyl	% quar-terphenyl	Thickness of sample at specified initial neutron energy
Ortho-terphenyl	98	1	1	0	0.025 in.–0.025 ev 0.025 in.–0.10 ev
Meta-terphenyl	1	94	5	0	0.025 in.–0.025 ev 0.025 in.–0.10 ev
Para-terphenyl	0	5	95	0	0.025 in.–0.025 ev 0.025 in.–0.10 ev
Santowax-R	9.0	52.4	30.3	8.3	0.0206 in.–0.010 ev 0.0206 in.–0.015 ev 0.0206 in.–0.025 ev 0.0257 in.–0.07 ev 0.0322 in.–0.10 ev

and β for use in reactor calculations were not successful because of the complex structure in the data.

B. EXPERIMENTAL PROCEDURE

The MTR phased-chopper velocity selector has been described in detail.[6] It consists of two slow neutron choppers spaced 3.4 meters apart and two rotating collimators to limit fast-neutron background, all spinning at 4935 rpm. With the desired rotor phase between the choppers, bursts of monoenergetic neutrons are produced. In scattering experiments these neutrons are scattered by the sample placed $\frac{1}{2}$ m after the second chopper and detected by sets of $B^{10}F_3$ counters 2 m away from the sample and at angles of 16.3, 26.0, 36.4, 47.6, 59.5, 72.1, and 84.7° to the initial beam. The time-of-flight of the neutrons from the sample to the detectors is determined by the 8192-channel analyzer using 10-μsec channel widths. The energy, time resolution, and flux of the incident neutrons are determined by a BF_3 counter or a fission chamber (called the beam monitor) placed at 2 m from the sample in the incident beam.

For each data run a sample at the desired temperature is placed in the sample changer at the sample position. Data is recorded automatically for 24 to 48 hr in 20-min cycles, 10 min of sample and 10 min of empty sample container. The sample and open data for the seven angles and beam monitor are then recorded, the open data is normalized if necessary to fit the sample data at small and large times for background subtractions, the initial energy and flux is determined from the beam monitor burst, and the data converted to partial differential cross sections and to the scattering-law presentation.

C. SAMPLES

The solid samples were made by casting slabs of the desired terphenyl, then machining the slabs to size. Table I gives the composition[15] of the solid samples and the thickness used for each initial energy. The thicknesses were adjusted to give about 10–20% scattering of the initial neutrons which allows ample counting rate, but limits the effects from multiple scattering. Each sample had sufficient length and width to cover the 4-×1.3-in. beam at the sample position. Each sample was held at its edges by double-faced masking tape to a thin cadmium-covered aluminum frame. This frame and sample were mounted in the sample position of the changer while an identical empty frame was mounted in the open position.

To hold the liquid Santowax-R, sample containers with 0.25-in.-wide aluminum frames holding 0.010-in.-thick aluminum windows were made. The windows had ample width and length to cover the 4-×1.3-in. beam, the frame being outside the beam area. A 192-w heating tape was wrapped around the frame and covered with cadmium. The heating coil was controlled by an upper level thermocouple control, the thermocouple of No. 28 wire being pushed down to the center of the sample container. The uncertainty in temperature from the range of control and from the nonuniform heating across the sample was about ±10°C. The thermocouples were checked against a stem-corrected glass-mercury thermometer. A similar heated sample container with thermocouple wire was placed in the open position.

The thickness of the terphenyl in the sample containers was about 0.032 in., but varied because of the heating, annealing, and stretching of the aluminum windows. Corrections for this effect were considered when the data were integrated and normalized to the total cross sections. These samples are thicker than desired, causing multiple scattering effects which are discussed later.

Distillation occurred during the course of the hot sample experiments causing enrichment in the higher boiling components. Table II gives the w% composition[15] of the samples before and after the experiments. The holder was cleaned and refilled between the two experiments. The lower temperature sample changed at a slower rate but changed more overall because the 207°C experiment took longer. It is assumed that these changes have little effect on the scattering data.

[15] J. C. Hillyer, Special Products Division, Phillips Petroleum Company, Bartlesville, Oklahoma (private communication).

TABLE II. Properties of liquid Santowax-R samples.

Sample	% ortho-terphenyl	% meta-terphenyl	% para-terphenyl	% quar-terphenyls	Thickness of sample (in.) at all initial neutron energies
Santowax-R before heating	9.0	52.4	30.3	8.3	
Santowax-R after 207°C experiment	4.4	49.3	30.4	15.9	~0.032
Santowax-R after 267°C experiment	5.6	54.5	33.6	6.3	~0.032

D. TOTAL CROSS SECTIONS

Total cross sections were measured for normalizing the scattering data. The beam of the velocity selector was collimated for these measurements to about 0.5 in. square and was detected by a $B^{10}F_3$ counter placed in the beam at about 2.5 m from the sample position. Samples of the solid terphenyls between 0.15 and 0.22 in. thick and a sample of the liquid Santowax-R about 0.187 in. thick were placed at the sample position. The transmissions were measured by oscillating sample and empty sample containers into the beam at 3-min intervals. The initial neutron energy at the peak of the burst was 0.0251 ev. Since the neutrons were in bursts, the time distributions allowed easy and accurate subtraction of the background. In 1-hr runs, about 14 000 sample counts and 35 000 open counts were obtained in the bursts.

Table III contains the total cross-section values. The errors include 1% for counting statistics and 3% for sample uncertainties (density, thickness, sample nonuniformities). A standard sample of gold was measured and agrees within 0.5% with previously measured values.[16]

The cross sections of the solid terphenyls increase slightly with decreasing melting point. The cross section of solid Santowax-R is within the experimental error of the weighted averages of the ortho-, meta-, and para-terphenyl cross sections. The cross section for liquid Santowax-R is lower than that for solid Santowax-R and decreases with increasing temperature.

TABLE III. Total cross sections per molecule of terphenyls at 0.0251 ev initial neutron energy.

Sample	Temperature (°C)	Total cross section
Ortho-terphenyl	23	911±27 barns/molecule $C_{18}H_{14}$
Meta-terphenyl	23	900±27 barns/molecule $C_{18}H_{14}$
Para-terphenyl	23	872±26 barns/molecule $C_{18}H_{14}$
Santowax-R	23	878±26 barns/molecule $C_{18}H_{14}$
Santowax-R	207	810±24 barns/molecule $C_{18}H_{14}$
Santowax-R	267	791±24 barns/molecule $C_{18}H_{14}$
Gold standard	23	106.9±1.0 barns/atom
Gold (previous measurement)[a]	23	106.4±0.2 barns/atom

[a] See reference 16.

[16] O. D. Simpson, N. H. Marshall, and R. C. Young, Nuclear Instr. and Methods (to be published).

E. SOLID TERPHENYL DATA

An example of the partial differential cross sections for scattering from solid Santowax-R is shown in Fig. 1. Similar results were obtained at other initial energies and for the ortho-, meta-, and para-samples. The cross sections are in units of barns per angstrom steradian for a terphenyl molecule $C_{18}H_{14}$. The figure in the upper left hand corner is the beam monitor burst shape and shows the time resolution of the incident beam. At the higher initial energies and forward angles, the distributions are only a little wider than the beam monitor. The effect of this resolution will be evident when the data are presented as scattering law. Since the raw data were smoothed by the "five-point smoothing,[1,6] the point fluctuation gives an indication of the counting statistics after smoothing.

The data in the scattering-law presentation $S(\alpha,\beta)$ for the solid Santowax-R at all initial energies are shown in Fig. 2. $S(\alpha,\beta)$ is per molecule. A value of mass M equal to one hydrogen mass is used in α, and a value of $\sigma_{\text{bound atom}}$ equal 81 barns is used to convert cross sections to $S(\alpha,\beta)$. Beta is in units of $K_BT=0.0255$ ev. Open points are for neutron energy loss and solid points for neutron energy gain. For each initial energy small scattering angles are to the left and large scattering angles to the right.

In the scattering-law presentation, energy gain, and energy loss points from different initial energies and angles for a single β value should form a single curve.[8] This is not true in Fig. 2. To understand the experimental discrepancies, first consider the effects of time resolution. As the initial energy increases or the scattering angle decreases, the width of the partial differential cross sections become increasingly narrower approaching the width of the beam monitor burst. The effect of this finite time resolution is to lower the peaks and raise the wings compared to their true values. Since $S(\alpha,\beta)$ intermixes data from different initial energies and angles, the resolution effects are most noticeable in this presentation. In Fig. 2, for $\beta=0$, the points for small scattering angles (left-hand side) fall below their corresponding points from larger scattering angles obtained at lower initial neutron energies. Each successively lower initial energy gives higher values. Taking these resolution effects into account, the best value of $S(\alpha,0)$ is a line through the envelope of points on the

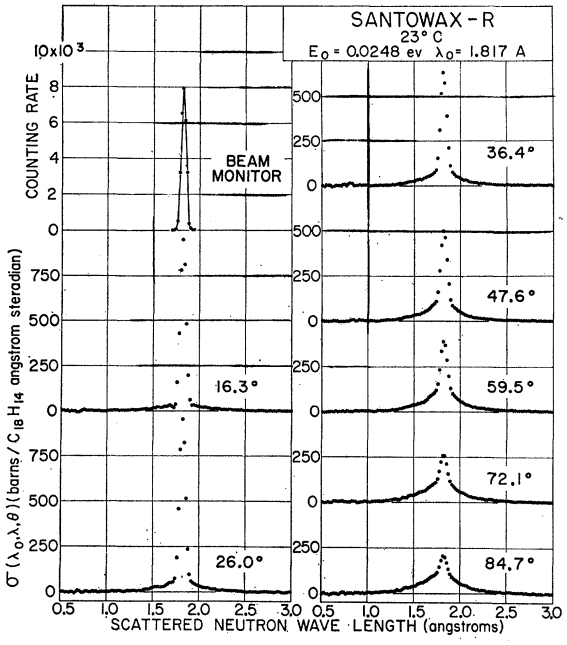

FIG. 1. Partial differential cross sections for scattering of 0.025 ev neutrons from room-temperature Santowax-R.

high $S(\alpha,0)$ side. The rounding of $S(\alpha,0)$ at low α may still be the effect of resolution, for which corrections are not evident, since data at lower energies were not obtained.

For $0.1 \leqq \beta \leqq 0.5$, the effects of the increase due to resolutions in the wings of the partial differential cross sections are evident. The points from small angles at large initial energies are above corresponding points at larger angles and lower initial energies. This is the filling in of the wings. The best values of $S(\alpha,\beta)$ at these β's is a line near the smaller values of $S(\alpha,\beta)$.

A third effect of finite resolution is that energy gain and energy loss points for the same β and from the same angle and initial energy do not fall on the one line. This effect, since it is relatively small and is not always in the same direction, is not obvious in the figures, being overshadowed by other errors.

As β increases, the energy loss data tend to lie consistently above the energy gain data. A probable cause of this splitting is multiple scattering. Estimates for the sample thickness used indicate that multiple scattering has more effect compared to the single scattering at the forward scattering angles at the large β values. Also, the observed discrepancies are of the magnitude estimated. Because the neutrons will migrate toward thermal and because the cross sections increase as incident energy decreases, multiple scattering causes neutron energy loss points to fall above neutron energy gain points.

A possible cause of the splitting is that when the open raw data distribution does not match the sample raw data distribution at short and long times, the open is normalized to the sample before subtracting to obtain

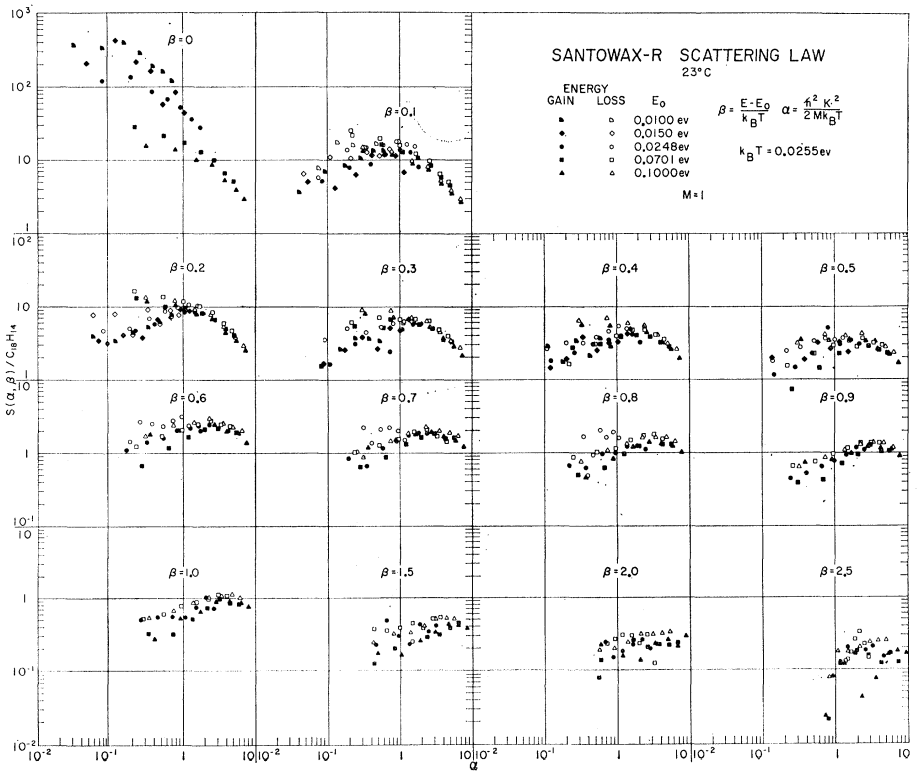

FIG. 2. Scattering law presentation of room-temperature Santowax-R data. M=one hydrogen atomic mass.

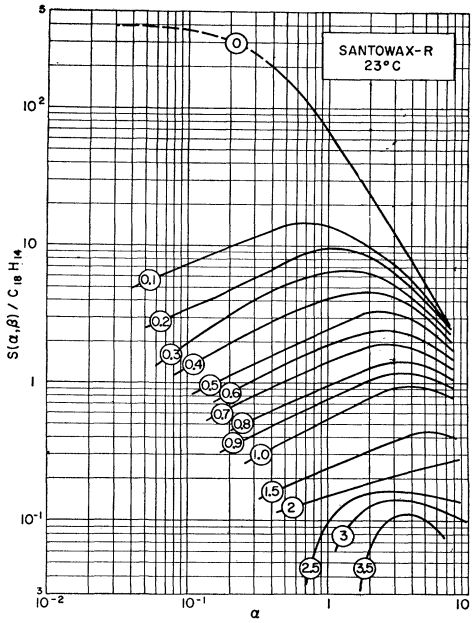

FIG. 3. Smooth scattering law curves for the room-temperature Santowax-R data.

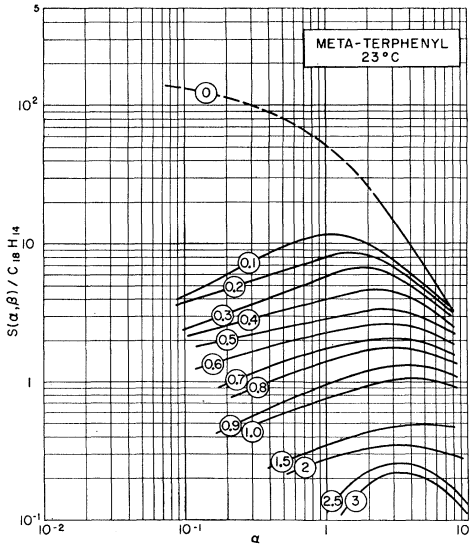

FIG. 5. Smooth scattering law curves for the room-temperature meta-terphenyl data.

the effects of the sample only. This normalization may be consistently in error and give the observed effects. However, this normalization is usually needed for the 0.1 and 0.07 ev initial neutron energy data, but not for the 0.025 ev and below data, and the 0.025 ev data still show the splitting effect.

Another possible cause of the disagreement between energy gain and energy loss points at high β values is an error in the temperature T of the sample or in the initial energy E_0 of the incident neutrons. However, discrepancies in T or E_0 needed to cause the splitting observed in the data are much larger than the estimated errors of T and E_0.

Multiple scattering is probably the major cause of this splitting at large β values. Considering the possible causes, the best value of $S(\alpha,\beta)$ at these higher β values is a line near the energy gain points. Applying the best estimates of multiple scattering and the effects of

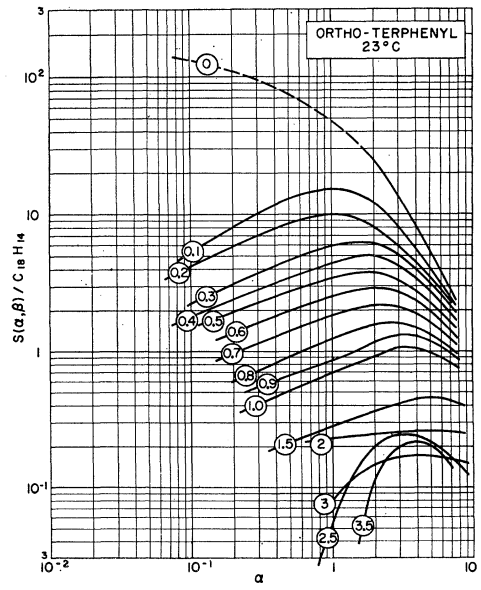

FIG. 4. Smooth scattering law curves for the room-temperature ortho-terphenyl data.

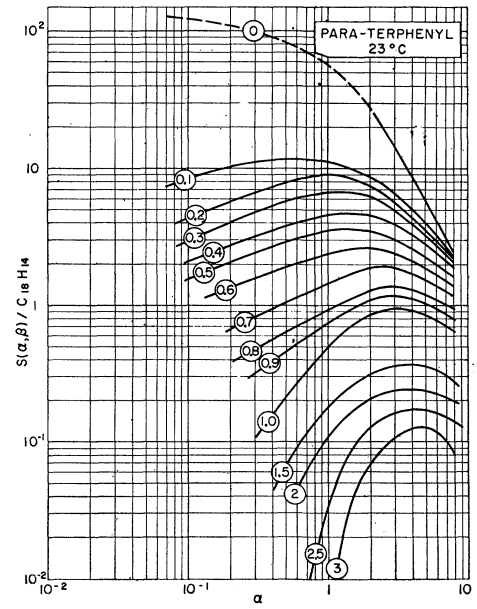

FIG. 6. Smooth scattering law curves for the room-temperature para-terphenyl data.

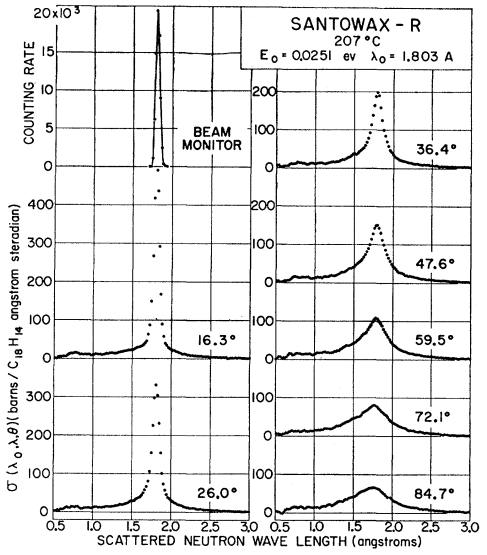

FIG. 7. Partial differential cross sections for scattering of 0.025-ev neutrons from 207°C Santowax-R.

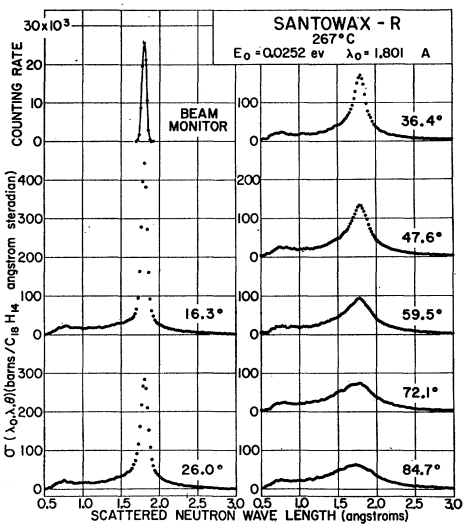

FIG. 8. Partial differential cross sections for scattering of 0.025-ev neutrons from 267°C Santowax-R.

resolution, curves have been drawn through the $S(\alpha,\beta)$ points. These curves for solid Santowax-R and for solid ortho-, meta-, and para-terphenyls are shown in Figs. 3–6. The dashed portion of the curves are in doubt because corrections were not made for resolutions in these portions. Lower initial energy data are needed to make these corrections.

F. LIQUID SANTOWAX-R DATA

Examples of the partial differential cross sections for scattering from liquid Santowax-R at 207° and

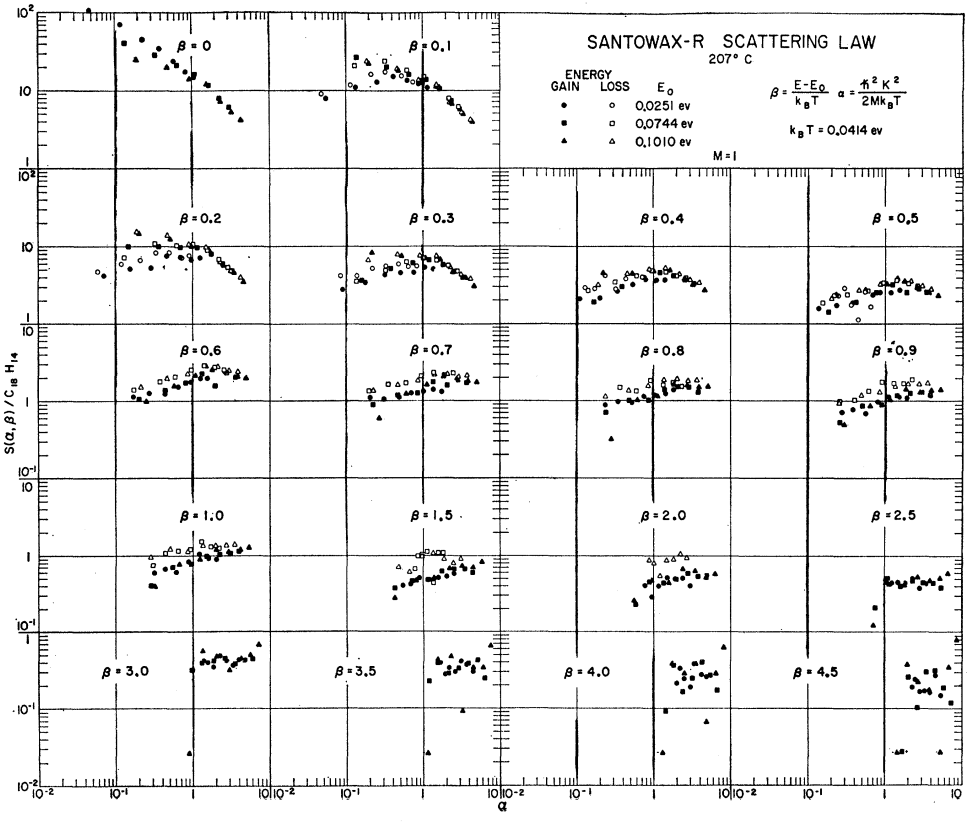

FIG. 9. Scattering law presentation of 207°C Santowax-R data. M =one hydrogen mass.

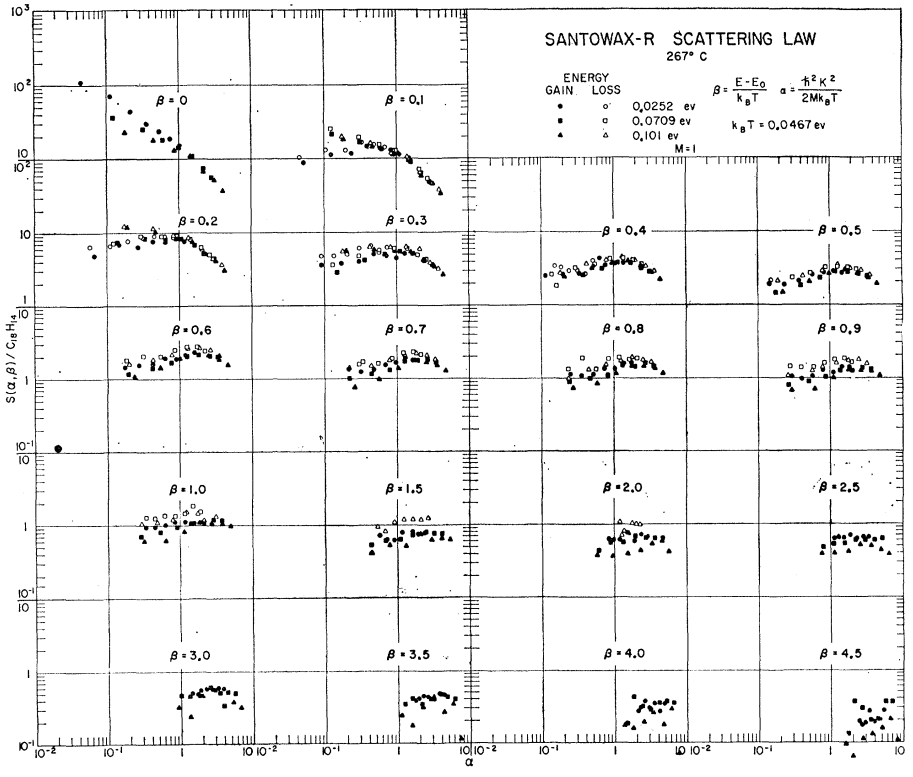

FIG. 10. Scattering law presentation of 267°C Santowax-R data. M=one hydrogen mass.

267°C are shown in Figs. 7 and 8. These data in the scattering law presentation are shown in Figs. 9 and 10, with β in units of K_BT=0.0414 and 0.0465 ev, respectively. The sets of smoothed curves are shown in Figs. 11 and 12. The liquid Santowax-R data compared to the solid Santowax-R data are less affected by resolution, because the distributions are broader. The liquid data are more affected by multiple scattering because the samples were thicker. Also, data at larger values of energy change were obtained because of the increased excitation of the sample.

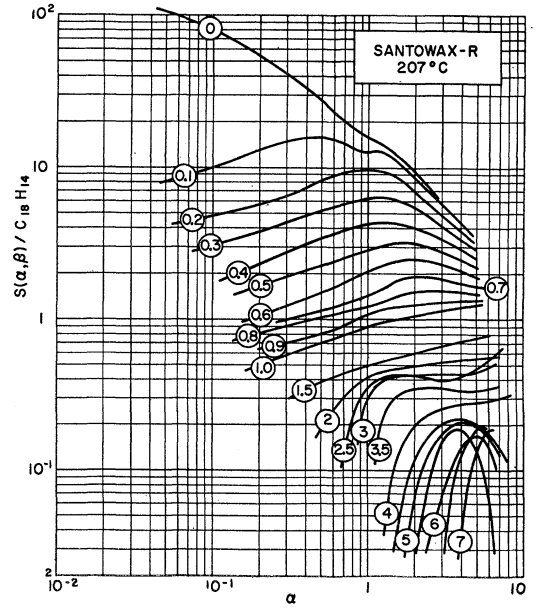

FIG. 11. Smooth scattering law curves for the 207°C Santowax-R data.

G. DISCUSSION

The scattering law presentations of the data of all the samples have similarities of shape. The β=0 curves continuously decrease in magnitude with increasing α. At small α's, for $0.1 \leqq \beta \leqq 2$ the curves all approach straight lines on the log-log plot and have about the same slopes. The straight line and the magnitude of the slope are similar to that found for H_2O and D_2O,[4,9] but the slope is about one-half that found for graphite.[5,9] A gas[1,2,9] does not have this straight line shape in a similar region of $S(\alpha,\beta)$ space.

At small α's and for $\beta \geqq 3$ the curves assume a shape similar to an ideal gas and decrease rapidly. The value of β at which this change from straight line to ideal gas shape occurs is nearly constant with sample being about β=3 (0.14 ev) for the 267° data, about β=2 (0.083 ev) for the 207° data, and about β=2.5 (0.065 ev) for the solid terphenyl data.

All of the curves for the solid terphenyls are similar in magnitude and shape. Differences are noted in comparing isolated β curves but differences that can be attributed to the ortho-, meta-, or para-binding are not

evident. The differences between isolated β curves can be due to the drawing of the curves through the data points. One exception is the meta-terphenyl curves in which the slope of the curves for $\beta \leqq 1$ at $\alpha > 2$ are consistently different from the ortho- or para-terphenyl or solid Santowax-R curves. It is not known why this happens.

For the solids at low α, the $\beta=0$ curve is 50 times the $\beta=0.1$ curve. In the partial differential cross section this appears as a very tall, sharp peak at $\Delta E=0$ sitting on a very broad base. This is similar to the water data reported by Brockhouse[17] and explained by a combination of simple diffusion and jump diffusion.

At small β's, the $S(\alpha,\beta)$ curves for liquid Santowax-R at 207° and 267°C are similar. For $\beta=0$, the 207°C curve lies higher. As β increases, the 207°C β curves decrease faster.

Resonance bands are observed in the infrared spectra of liquid Santowax-R at 0.087, 0.093, 0.10, 0.104, 0.110, and 0.125 ev.[15] Resonances of 0.05 and 0.09 ev have been observed in the scattering of cold neutrons,[18] and in infrared,[19] and in Raman[20] spectra from samples of liquid benzene. The transitions most probably observed in inelastic scattering experiments are those with large amplitude of hydrogen motion.[21] Not all of the above-mentioned resonance bands are associated with vibrations having large hydrogen amplitudes. Similarly there may be transitions having large hydrogen amplitudes that are not observed in the infrared and Raman spectra. The solid Santowax-R data did not extend to large enough β values to observe most of the above-mentioned transitions. The 0.05-ev ($\beta=2$) transition was not evident. The resonances at 0.1 and 0.2 ev in the liquid data are probably due to one or more of these resonance bands but it is not possible to select a precise transition. The resonances produced by discrete transition in inelastic scattering are broadened to such an extent by the thermal motion of the molecules that precise energies are difficult to determine.

Comparing the liquid and solid Santowax-R curves, for $\beta=0$ the solid curve is 20 to 50 times higher. Also, this solid curve increases more rapidly than the liquid $\beta=0$ curves as α decreases. For $\beta>0$ the solid curves decrease more rapidly with β than do the liquid curves.

H. CLASSIFICATION OF SCATTERING-LAW CURVES

From a comparison of the available $S(\alpha,\beta)$ data,[9] the curves appear to fall into three classes: (1) poly-

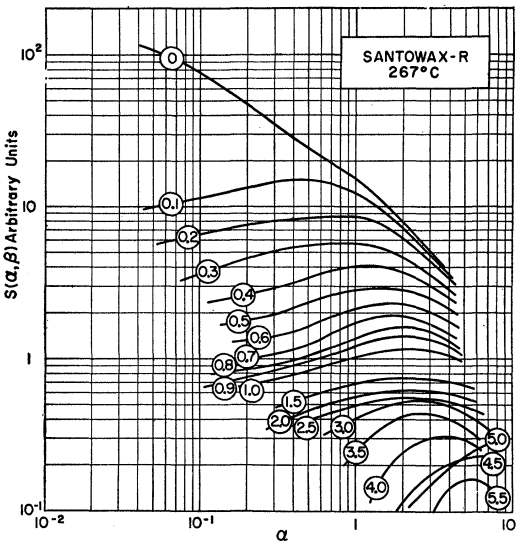

FIG. 12. Smooth scattering law curves for the 267°C Santowax-R data.

crystalline solids, (2) liquid–amorphous solids, and (3) gases. The $S(\alpha,\beta)$ curves for methane[1] and propane[2] gas have the general shape of an ideal gas; for $\beta>0$ at α values below the broad peak, the slope of the curves on the log-log plot continuously increases as α decreases. The $S(\alpha,\beta)$ curves for class two (H_2O, D_2O[4], liquid and solid Santowax-R) are characterized by a slope of one-half on the log-log plot for α's below the broad peak and for $0.1 \leqq \beta \leqq 3$. The $S(\alpha,\beta)$ curves for class one (graphite[5]) are characterized by a slope of one on the log-log plot for α's below the broad peak and for $0.1 \leqq \beta \leqq 3$. The terphenyls appear to fit into the second class with H_2O and D_2O.

I. FOURIER TRANSFORMATION OF $S(\alpha,\beta)$

The incoherent partial differential cross section is the double Fourier transformation of the Van Hove[11] space-time self-correlation function $G_s(\bar{r},t)$ and some theoretical predictions of this function have been made.[13] The terphenyl data were not double Fourier transformed to obtain $G_s(\bar{r},t)$, as Brockhouse did his liquid lead data,[3] because of the limited extent and accuracy of the terphenyl data and because no predicted $G_s(\bar{r},t)$ for these complex samples were available.

The Egelstaff method[4,7,12] of extrapolating $S(\alpha,\beta)/\alpha$ to $\alpha=0$ in order to obtain a function related to the velocity correlation function was not pursued because of the difficulty of making these extrapolations. To extrapolate $S(\alpha,\beta)/\alpha$ to $\alpha=0$ on a linear scale, $S(\alpha,\beta)$ in the log-log presentation must be a line with a slope greater than 45°. If the slope is less than 45°, as is the terphenyl data, $S(\alpha,\beta)/\alpha$ goes to infinity as α goes to 0. Egelstaff proposes that, in cases where difficulty is encountered in extrapolating, trial theoretical curves be fit to the $S(\alpha,\beta)$ data in particular regions to guide

[17] B. N. Brockhouse, *Proceedings of the Varenna Conference on the Condensed State of Simple Systems, Varenna, 1957* [Suppl. Nuovo cimento **9**, 45 (1958)]; Acta Cryst. **10**, 827 (1957).
[18] V. W. Myers, M. J. Cotter, and H. Palevsky, Bull. Am. Phys. Soc. **6**, 262 (1961).
[19] American Petroleum Institute Infrared Spectra Compilation by API Research Project 44, Carnegie Institute of Technology, Pittsburgh.
[20] G. Herzberg, *Infrared and Raman Spectra* (D. Van Nostrand Company, Princeton, New Jersey, 1945).
[21] H. L. McMurry (private communication).

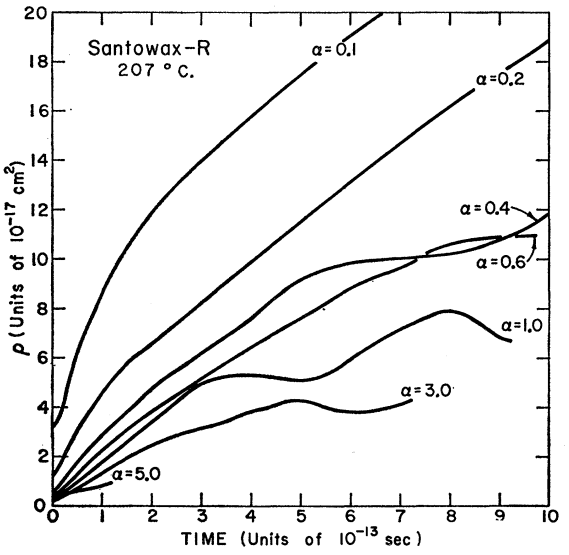

FIG. 13. $\rho(t)$'s vs time obtained by Fourier transforming the data of Fig. 11.

the extrapolation. No theoretical $S(\alpha,\beta)$ curves were available that matched the shape of the terphenyl data at small α. The fitting of trial theoretical curves to the data for larger α as a guide for extrapolating $S(\alpha,\beta)/\alpha$ to $\alpha=0$, past the region where the trial curves do not fit, is questionable. This fitting appears to disregard part of the experimental data and to introduce preconceived ideas into the interpretation. Therefore this method was not pursued. If such an extrapolation were successful, then a function related to the velocity correlation function or a width $\rho(t)_{\alpha=0}$ (defined in the next paragraphs) could be obtained.

Vineyard[13] has shown in the classical limit that for idealized materials such as the perfect gas, the diffusing atom, the oscillator, and the Debye solid, the self-correlation function $G_s(\bar{r},t)$ can be written as a Gaussian function, $\exp[-r^2/2\rho(t)]$, where $\rho(t)$ is a function of time only. Vineyard showed that applying Fourier inversions to the Gaussian correlation function gives

$$\rho(t)=\frac{2}{\kappa^2}\ln\left(\frac{4\pi\hbar}{\sigma_{\text{bound atom}}}\int_{-\infty}^{\infty}\frac{k_0}{k}e^{+i\omega t}\frac{d^2\sigma}{d\Omega dE}d\omega\right). \quad (1)$$

The $\rho(t)$, if it is independent of κ, is overdetermined by Eq. (1) and an important check on the assumptions made is to apply Eq. (1) for several different values of κ to see if the same function $\rho(t)$ is obtained for each. However, for the terphenyl data the classical limit is not valid.

To consider the problem quantum mechanically and in terms of scattering law, $S(\alpha,\beta)=[4\pi/\sigma_{\text{bound atom}}]\times[k_0/k][\exp(+\beta/2)][K_BT][d^2\sigma/dEd\Omega]$ was substituted into the quantum mechanical equivalent of Eq. (1),[13,14] to obtain

$$\rho(t)=\frac{\hbar^2}{MK_BT\alpha}\ln\left(\int_0^{\infty}\cos(\omega t)S(\alpha,\beta)d\beta\right). \quad (2)$$

Replacing $e^{i\omega t}$ by $\cos(\omega t)$ is justified because $S(\alpha,\beta)$ is even in β. If the assumptions are correct, identical values of $\rho(t)$ will be obtained by applying Eq. (2) at different values of α. Also the $\rho(t)$ can be compared to the proposed $\rho(t)$ of Rahman.[14]

Vineyard mentions that $d^2\sigma/d\Omega dE$ must be properly normalized before applying Eq. (1). The scattering length for hydrogen is much larger than the scattering length for carbon; hydrogen is the principal scatterer in terphenyls and the $S(\alpha,\beta)$ inserted in Eq. (2) should be per hydrogen atom. Thus the data of Figs. 3–6 and 11 and 12 were normalized by 1/14 before trying to determine $\rho(t)$. If the data are improperly normalized, the ordinates of $\rho(t)$ for one value of α will be shifted compared to the ordinates of $\rho(t)$ at another value of α.

A computing machine program was written that solves Eq. (2) at given α for data of the form of Figs. 3–6 and 11 and 12. Also, a program was written to perform the inverse of Eq. (2) having obtained $\rho(t)$. Testing these programs using the theoretical ideal gas $S(\alpha,\beta)$,[9] a single $\rho(t)$ curve was obtained for $\alpha=0.1$, 1, and 5. This $\rho(t)$ curve agreed with the analytical $\rho(t)=\text{const}\times(\frac{1}{4}+t^2)$. Using this $\rho(t)$, the second machine program inverted to the original $S(\alpha,\beta)$ curves. These computations showed that the programs are working correctly and the calculations are sufficiently accurate. Applying Eq. (2) to the methane data[1] normalized by $\frac{1}{4}$ (to change to the value per hydrogen atom) at α's between 0.1 and 5, a single $\rho(t)$ was not obtained. Better agreement was obtained when $S(\alpha,\beta)$ was normalized by 0.28 but still a single curve was not obtained. Also, the $\rho(t)$'s did not have the shape characteristic of an ideal gas.

Applying Eq. (2) to $(1/14)S(\alpha,\beta)$ for the 207°C Santowax data at α's between 0.1 and 5, a single $\rho(t)$ was not obtained. Examples of these $\rho(t)$'s are shown in Fig. 13. The disagreement is not a simple shift of ordinates caused by an improper normalization. At larger α's, the curves intercept the ordinate near the value of 0.26×10^{-17} cm² as is predicted for quantum substances.[14] At small α's the $\rho(t)$'s are much too high. The $\rho(t)$'s at large α could not be determined at large times because of the limited extent and accuracy of the data. Some of the fluctuations and variations of the $\rho(t)$ curves are due to the errors in the data but the large differences between curves and oscillations in some of the curves are larger than expected from experimental error. Similar sets of curves were obtained for the other sets of terphenyl data.

For 207°C Santowax-R, improvement in the agreement between $\rho(t)$'s was not achieved by changes in the normalization. Improvements were achieved by letting $\alpha\rho=\alpha^{\frac{1}{2}}\rho(t)_1$ or $\alpha\rho=(1+\alpha)\rho(t)_2$. Using $\alpha^{\frac{1}{2}}\rho(t)_1$ and $(1+\alpha)\rho(t)_2$ in place of $\alpha\rho(t)$ in the inversion program to

obtain $S(\alpha,\beta)$ showed that, $\alpha^{\frac{1}{2}}\rho(t)_1$ gives better agreement at small α's and $(1+\alpha)\rho(t)_2$ gives better agreement at large α's. In these inversions, $\rho(t)_1$ and $\rho(t)_2$ were the best single line drawn through all of the curves. As seen from Fig. 13, a single curve could not be obtained for the $\rho(t)$ case. In the $(1+\alpha)\rho(t)_2$ case, the $\rho(t)_2$ term is a normalizing factor. The width functions $\rho(t)_1$ and $\rho(t)_2$ do not have the shape of $\rho(t)$ for an ideal gas. At small α's the $\alpha^{\frac{1}{2}}\rho(t)_1$ gives the $S(\alpha,\beta)=a(\alpha^{\frac{1}{2}})+b$ shape (a and b are constants). It does not give the change from $S(\alpha,\beta)=a(\alpha^{\frac{1}{2}})+b$ to the ideal gas shape at $\beta\cong 2.5$.

For the terphenyls and also for methane one concludes that $\rho(t)$ of Eq. (2) is not a function of time only but that it is also a function of momentum change and $G_s(\bar{r},t)$ is therefore not Gaussian. This is not unexpected since the proposed theory assumes translational motions only and does not consider molecular rotational and vibrational transitions. This transformation was attempted in hopes that the variations from Gaussian would be small or that possible modifications would become evident.

J. MODERATING PROPERTIES OF SANTOWAX-R

Santowax-R is used as the moderator-coolant in several power reactors. The advantages are that these reactors can operate at low pressure but at high temperature and thus high thermal efficiency. An estimate of the moderating quality of Santowax-R can be obtained by comparing the $S(\alpha,\beta)$ for Santowax-R to that for water which is accepted as a good moderator. Since the only available H_2O $S(\alpha,\beta)$ data for water is at 150°C,[9] the 207°C Santowax-R data converted to $S(\alpha,\beta)$ per hydrogen atom was compared with it. The water and the Santowax-R curves have similar shapes and similar magnitudes. At any α, the β curves fall off at about the same rate of energy loss. The difference is that Santowax-R does not have as steep a slope for large α's on the log-log plot. This comparison shows that Santowax-R is a good moderator per hydrogen atom. The disadvantage is that the hydrogen density of Santowax-R is about half that for water.

From the shapes of the $S(\alpha,\beta)$ curves, liquid Santowax-R is a better moderator at the higher temperature because of the higher cross section per neutron for energy exchange. Solid Santowax-R has less energy exchange than the liquid. At very low α values, energy exchange becomes improbable.

K. SUMMARY AND CONCLUSIONS

From comparisons of the data for the six different samples, it is found that (1) no effect of the ortho-, meta-, or para-chemical binding is evident, (2) the liquid and solid data have similarities of shape but are different in magnitude, and (3) resonances caused by discrete energy transitions are observed in the liquid data, but not in the solid data. Comparison per hydrogen atom between the inelastic scattering for water and for liquid Santowax-R shows that Santowax-R is an effective thermal moderator.

The terphenyl data combined with other sets of data that are becoming available allow similarities to be seen in the scattering law presentations. From these similarities classes of materials may be postulated. The scattering law of the terphenyls, both solid and liquid, are similar to those of water and D_2O and are classed as liquid–amorphous solid, while graphite is classified a polycrystalline solid and methane and propane gas are classified gases. More data for more samples in the scattering law form are needed to justify this postulate of classes.

ACKNOWLEDGMENTS

The author wishes to acknowledge the data processing of Mrs. C. J. Slayden, many helpful discussions with and assistance from Dr. H. L. McMurry, Dr. G. W. Griffing, Dr. P. D. Randolph, Dr. R. E. Schmunk, and Mr. K. A. Strong, and the advice and encouragement of Dr. R. G. Fluharty.